END
DATE
FILMED

11-80

DTIC

1.0

1.1

1.25   1.4   1.6

45   2.8   2.5

3.2   2.2

3.6

4.0   2.0

1.8

MICROCOPY RESOLUTION TEST CHART

NATIONAL BUREAU OF

LEVEL

AN ANALYTICAL APPROACH FOR USE WITH WAVEGUIDE ENZYME-INACTIVATION INVESTIGATIONS

By

Johnson J. H. Wang

The findings in this report are not to be construed as an official
Department of the Army position unless so designated by other
authorized documents.

DECEMBER 1978

GEORGIA INSTITUTE OF TECHNOLOGY

Engineering Experiment Station
Atlanta, Georgia 30332
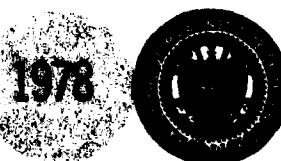
1978

80 10 3 121

REPORT DOCUMENTATION PAGE		READ INSTRUCTIONS BEFORE COMPLETING FORM
1. REPORT NUMBER	2. GOVT ACCESSION NO. AD-A090491	3. RECIPIENT'S CATALOG NUMBER
4. TITLE (and Subtitle) An Analytical Approach for Use with Waveguide Enzyme-Inactivation Investigations		5. TYPE OF REPORT & PERIOD COVERED Final Report. Feb 77 – Sep 78
		6. PERFORMING ORG. REPORT NUMBER
7. AUTHOR(s) J. J. H. Wang		8. CONTRACT OR GRANT NUMBER(s) DAMD17-77-G-9422
9. PERFORMING ORGANIZATION NAME AND ADDRESS Engineering Experiment Station Georgia Institute of Technology Atlanta, Georgia 30332		10. PROGRAM ELEMENT PROJECT, TASK AREA & WORK UNIT NUMBERS (62771A), 3E762771A805, 00.003), (61102A), 3M161102BS01 00.116)
11. CONTROLLING OFFICE NAME AND ADDRESS Army Medical Research and Development Command Fort Detrick, Frederick, MD 21701		12. REPORT DATE 1 December 1978
		13. NUMBER OF PAGES 48 pages
14. MONITORING AGENCY NAME & ADDRESS(if different from Controlling Office)		15. SECURITY CLASS. (of this report) UNCLASSIFIED
		15a. DECLASSIFICATION DOWNGRADING SCHEDULE

16. DISTRIBUTION STATEMENT (of this Report)

Approved for Public Release; Distribution Unlimited

17. DISTRIBUTION STATEMENT (of the abstract entered in Block 20, if different from Report)

Approved for Public Release; Distribution Unlimited

18. SUPPLEMENTARY NOTES

19. KEY WORDS (Continue on reverse side if necessary and identify by block number)

Waveguide Discontinuity   Method of Moments
Dosimetry
Dyadic Green's Function
Microwave Enzyme Inactivation

20. ABSTRACT (Continue on reverse side if necessary and identify by block number)

A numerical analysis technique has been developed to compute the fields inside a three-dimensional arbitrarily-shaped heterogeneous dielectric or biological body inside a rectangular waveguide. The numerical computation involves a dyadic Green's function containing a double infinite series, which is evaluated by a partial summation technique. The numerical results compared —

DD FORM 1473 EDITION OF 1 NOV 65 IS OBSOLETE

very well with reflection and thermographic measurements. This analytical approach should be an efficient tool in guiding the design of microwave applicators used for rapid inactivation of enzymes.

Acces		
NTIS		
DTIC		
Unann		
Justi		
By		
Distr		
Aval		
Dist		

AN ANALYTICAL APPROACH FOR USE WITH WAVEGUIDE

ENZYME-INACTIVATION INVESTIGATIONS

FINAL REPORT
PROJECT A-1943

By

Johnson J. H. Wang

December 1, 1978

Georgia Institute of Technology
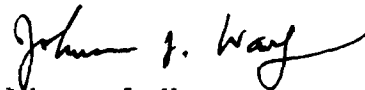Atlanta, Georgia 30332

SUMMARY

A numerical analysis technique has been developed to compute the
fields inside a three-dimensional arbitrarily-shaped heterogeneous
dielectric or biological body inside a rectangular waveguide. The
numerical computation involves a dyadic Green's function containing a
double infinite series, which is evaluated by a partial summation
technique. The numerical results compared very well with reflection and
thermographic measurements, which were conducted at Walter Reed Army
Institute of Research. This analytical approach should be an efficient
tool in guiding the design of microwave applicators used for rapid
inactivation of enzymes. In addition, the accomplishment represents a
significant progress in microwave and electromagnetic theory.

FOREWORD

The research on this grant was carried out by the Electromagnetic Effectiveness Division of the Systems and Techniques Laboratory of the Engineering Experiment Station at the Georgia Institute of Technology, Atlanta, Georgia 30332. Dr. Johnson J. Wang served as the Principal Investigator. Experimental work in this research was performed at Walter Reed Army Institute of Research under the supervision of Dr. Lawrence E. Larsen. This report covers the work which was performed from 1 February 1977 to 30 September 1978.

The author wishes to express his gratitude to Dr. Larsen for his experimental work and consultations, and to Mr. Fred L. Cain of Georgia Tech for his continuous interest and support.

Respectfully submitted,

Johnson J. Wang
Project Director

Approved:

Fred L. Cain
Chief,
EM Effectiveness Division

ii

TABLE OF CONTENTS

LIST OF FIGURES

SECTION I

INTRODUCTION

The role of cyclic adenosine monophosphate (cyclic AMP) as an intracellular mediator of the action of a number of hormones has been well established [1-3]. In addition, cyclic AMP is also considered important in the function of the central nervous system [4,5]. The distribution of cyclic AMP in the brain can therefore be used as an important tool in neurochemical research such as in the evaluation of the effects of hormones or drugs in the central nervous system. In order to determine the distribution of cyclic AMP, however, it is necessary to inactivate rapidly two enzymes, adenylate cyclase (AC) and phosphodiesterase (PDE), which produce and degrade cyclic AMP, if left active. Otherwise, the level of cyclic AMP concentration to be studied may be distorted in a few seconds after the animal is sacrificed [6-8].

There are two types of widely-used inactivation techniques -- liquid nitrogen freezing and microwave heating. The disadvantages of liquid nitrogen freezing include the slowness of the process, the nonuniformity of the freezing pattern throughout the brain [9,10], and the inconvenience in post-mortem dissection at freezing temperatures. Microwave heating is a promising approach based on the principle that cyclic AMP is a relatively heat-stable substance [11] while the AC and PDE enzymes are heat labile and denature irreversibly at temperatures in the range of 65°-90° C. With microwave heating, the inactivation of enyzmes can often be achieved with exposure times on the order of 1-2 seconds or less, permitting subsequent required dissection of the brain at room temperature.

Microwave inactivation can be carried out by an open or closed system. In the open system, a plane wave is employed to illuminate the animal without the direct interference of enclosing conducting boundaries. The disadvantages of the open system include a large power source required and the necessity of containment of radiated power with a conducting screen or an anechoic chamber. The closed system, such as

1

a rectangular waveguide, is highly efficient in power usage and has negligible leakage power which is desirable as far as radiation hazard and man-made noise are concerned. As a result, recent research in microwave inactivation techniques has been concentrated in the closed system type, such as the rectangular waveguide applicator [12]. Lenox, et al., [12] have shown that using a waveguide applicator, modified from a WR430 waveguide, only 2.8 seconds are needed to inactivate the brain enzymes in a 325-gram rat at 2450 MHz with a source of 3500 watts. Microwave leakage is less than 5 mW/cm^2 at a distance of 10 cm from the applicator surface.

Microwave heating can be considered as being generated by a continuously distributed equivalent source throughout the whole biological body, and is therefore potentially more uniform than the usual exterior heating produced by localized sources. The uniformity of temperature in a biological body under microwave excitation is determined by the degree of uniformity of the equivalent source distribution, its thermal conductivity, and the time of exposure. For the case of rapid enzyme inactivation, the heating pattern is roughly proportional to the equivalent source distribution. Therefore, nonuniform equivalent source distribution generates "hot spots" in the brain tissue, which may distort the AMP distribution to be studied. Difficulties in obtaining uniform heating patterns have long been recognized at Walter Reed Army Institute of Research (WRAIR) in its continued research effort in microwave enzyme inactivation [12].

The physical problem of waveguide enzyme inactivation is considerably more complex than the open inactivation system employing a plane wave. The physical parameters involved in the process are numerous, making it extremely difficult and expensive to design a waveguide inactivation system by a purely experimental or trial-and-error approach. Under these circumstances, the idea of guiding the design of the microwave applicator by an analytical approach appears attractive, and the present research grant was awarded to Georgia Tech to investigate the potentiality of this approach.

The theoretical approach taken at Georgia Tech was to develop a computer algorithm to compute the distribution of dissipated power

inside a three-dimensional arbitrarily-shaped heterogeneous dielectric body inside a rectangualr waveguide with matched termination. The theoretical work supported by this grant has been partially documented in a paper [13] which discussed the theory and its numerical validation. This analytical technique was then checked against thermographic data generated at WRAIR. Satisfactory agreements between the theoretical results and the thermographic data were observed.

The results of this research have demonstrated that the analytical approach taken at Georgia Tech is a powerful tool which should help significantly future development of a waveguide enzyme inactivation system to achieve rapid and uniform heating in the brain tissue. The technical accomplishments are discussed in the following sections together with recommendations for further research in this area.

SECTION II

THEORY

The problem to be considered is shown in Figure 1, in which a three-dimensional, arbitrarily-shaped heterogeneous biological body is electromagnetically illuminated in a rectangular waveguide. It is desired to determine the temperature distribution in the biological body as a function of space and time. The analysis involves two steps, namely, the computation of the distribution of power dissipation and the calculation of the resulting temperature distributions. The first step involves the solution of an electromagnetic boundary-value problem. The second step involves the solution of the heat conduction problem with the heat source represented by an equivalent distributed source of dissipated power density.

Although numerous publications have appeared in the literature on the analysis of waveguide discontinuity problems, not a single truly three-dimensional solution has been published, according to a review paper by Silvester in 1974 [14]. In the related cavity resonator problem, finite-element [15] and TLM [16] methods have been employed to compute the resonant frequency and field distribution when dielectric blocks were placed inside the cavities. Thus, the theoretical work performed in the present grant represents a significant advance in microwave and electromagnetic theory. Most of the details of the numerical analysis have been discussed in a publication [13] which is included in this report as an appendix. However, the treatment of the singular problem in the dyadic Green's function was only briefly mentioned in Reference 13. Because of the controversy in the literature on the singularity problem [17-22], it is desirable to document the approach taken for this problem in the present study.

The heat conduction analysis that relates the equivalent distributed source in the form of distributed power dissipation to the temperature distribution in the brain tissue has been carried out by Guy [23,24]. His approach was taken with modifications to explain phenomena
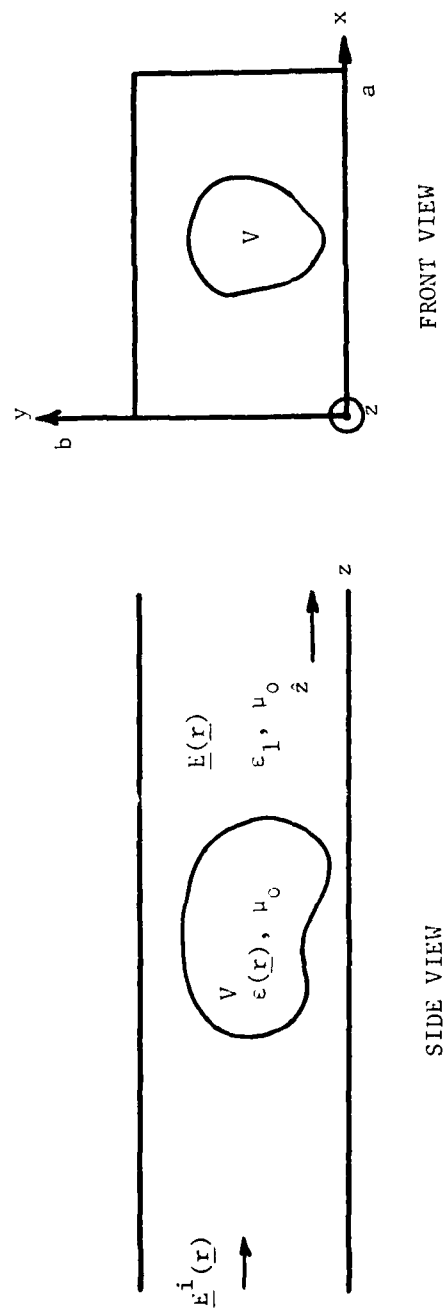
4

Figure 1. A three-dimensional arbitrarily-shaped biological body in a rectangular waveguide.

5

near the interface of thermal discontinuities.

A. The Electromagnetic Boundary-Value Problem

The basic approach has been summarized in Reference 13 which is included in the Appendix. In this report, the discussion will be restricted to the handling of the numerical difficulties in the singular and doubly-infinite series Green's function employed in the analysis.

Yaghjian [17,18] recently indicated that the dyadic Green's function in the source region was not unique but rather dependent on the geometry of the "principal volume" involved. This general statement, regardless of the boundary-value problem under consideration, was supported by Chen [25] for the free-space case. Their views offered an explanation for the apparent discrepancies in the literature [19-22] but are puzzling on some other aspects. In this report, no attempt is made to resolve the disputes conclusively but merely to provide information obtained in the present analysis which could be used by interested researchers.

The electric field in the source region, as shown in Figure 2, can be expressed in terms of a dyadic Green's function in the following form

$$\underline{E}(\underline{r}) = j\mu\omega \lim_{\Delta V \to 0} \int_{V - \Delta V} \underline{\underline{G}}(\underline{r},\underline{r}') \cdot \underline{J}(\underline{r}')dv' + \underline{E}_c(\underline{r}), \qquad (1)$$

where $\underline{r},\underline{r}'$ = positional vectors of the field and source points,

$\underline{\underline{G}}_e(\underline{r},\underline{r}')$ = the electrical dyadic Green's function,

$G_e(\underline{r})$ = electric field at $\underline{r}$,

$\underline{J}(\underline{r}')$ = source current at $\underline{r}'$,

ω = radian frequency,

μ = permeability in space S,

V = volume occupied by the volume current source,

ΔV = an infinitesimal volume in V enclosing the singularity of $\underline{\underline{G}}_e(\underline{r},\underline{r}')$ at $\underline{r} = \underline{r}'$, and

$\underline{E}_c(\underline{r})$ = a correction term.

The space S under consideration can be an infinite homogeneous space or a homogeneous space partially or completely bounded. The
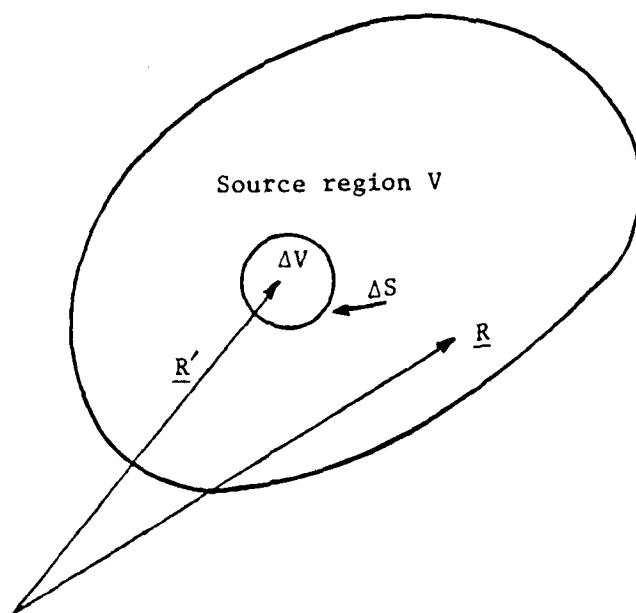
6

Figure 2. "Principal Volume" integration in the source region.

limiting term is often called the principal value of the integral since its singular point has been excluded. Discussions on the correction term and the principal-value integration dated back to the work of Kellogg [26]. The work of Kellogg and Van Bladel [27] implied that $\underline{E}_c$ was unique and independent of the choice of ΔV. In treating the principal integral of the scalar potential, Kellogg explicitly stated on page 18 that a necessary and sufficient condition for the convergence of the integral is that for any small positive number ε there exists a number $\delta > 0$ such that if ΔV and $\Delta V'$ are any two regions containing the singularity P and contained in the sphere of radius δ about P,

$$\left| \int_{V-\Delta V} - \int_{V-\Delta V'} \right| < \varepsilon . \tag{2}$$

Kellogg further emphasized that "the limit" is not regarded as existing if it is necessary to restrict the shape of ΔV in order to obtain a limit. The only restrictions on ΔV are that it shall have a boundary of a certain degree of smoothness (be a regular region in the sense of Chapter IV, Section 8, p. 100) that it shall contain P in its interior, and that its maximum chord shall approach 0. Spheres, circular cylinders, cubes, and pill boxes all have regular surfaces, and the resulting $\underline{E}_c$ in Equation (1) should therefore be also independent of the shape of ΔV, even though a vector, instead of a scalar, is involved.

In the present waveguide analysis, ΔV is chosen to be a rectangular-sided cell whose dimension along the longitudinal axis of the waveguide approaches zero while dimensions in the other two coordinates remain constant. This selection of principal volume ΔV appears to be the same as the "pill box" type in Yagjian's report [18], and is therefore in agreement with all the known views in the literature. However, numerical experiments have not yet been conducted to determine whether the correction term $\underline{E}_c$ is dependent upon the shape of the principal volume ΔV.

The self-impedance matrix element $Q_{\ell q}^{pp}$, which corresponds to the limiting integral on the right-hand side of Equation (1), should hold the answer to the present puzzle. Since the electric field $\underline{E}(\underline{r})$ is unique, the two terms on the right-hand side of Equation (1) must add up to yield the correct value for $\underline{E}(\underline{r})$. One can therefore construct various principal volumes to see whether a dependence on the principal volume exists for the correction term $\underline{E}_c$, and, if it does, whether a generalization as claimed by Yagjian [18] is valid. Even though no formal investigation has yet been made in this respect, an examination of the mathematical expressions in the waveguide case [13], the free space case [28], and the strict convergence criterion of Equation (2) indicates that the issue is far from being resolved.

The self-impedance element $Q_{\ell q}^{pp}$, for $p = 1$, can be evaluated by a partial summation technique as follows:

$$Q_{\ell q}^{11} = T_{\ell q}^{11} + S_{\ell q}^{11} , \tag{3}$$

where

$$T_{\ell q}^{11} = \frac{j}{2abk^2} \sum_{m=0}^{\infty} \sum_{n=0}^{\infty} \frac{\varepsilon_{on}\varepsilon_{om}}{k_{nm}} \left[\left(\frac{m\pi}{b}\right)^2 + k_{nm}^2 \right] \frac{4ab}{n\pi m\pi}$$

$$\left[\sin \frac{n\pi\Delta X_\ell}{2a} \sin \frac{m\pi\Delta Y_\ell}{2b}\right] \frac{2}{jk_{nm}} \cos\left[k_{nm}(Z_q - Z_\ell)\right]$$

$$\exp\left(jk_{nm}\Delta Z_\ell/2\right) \cos \frac{n\pi X_q}{a} \cos \frac{n\pi X_\ell}{a} \sin \frac{m\pi Y_q}{b} \sin \frac{m\pi Y_\ell}{b} , \tag{4a}$$

and

$$S_{\ell q}^{11} = \frac{-j}{2abk^2} \sum_{m=0}^{\infty} \sum_{n=0}^{\infty} \frac{\varepsilon_{on}\varepsilon_{om}}{k_{nm}} \left[\left(\frac{m\pi}{b}\right)^2 + k_{nm}^2 \right] \frac{4ab}{n\pi m\pi}$$

$$\left[\sin \frac{n\pi\Delta X_\ell}{2a} \sin \frac{m\pi\Delta Y_\ell}{2b}\right] \frac{2}{jk_{nm}} \cos \frac{n\pi X_q}{a} \cos \frac{n\pi X_\ell}{a}$$

$$\sin \frac{m\pi Y_q}{b} \sin \frac{m\pi Y_\ell}{b} , \tag{4b}$$

9

and all the notations are the same as defined in Reference 13.

The term $T_{\ell q}^{11}$ in Equation (3) converges rapidly but the term $S_{\ell q}^{11}$ converges extremely slow. Using the summation formulas in [13] one obtains

$$
S_{\ell q}^{11} = \frac{1}{k^2\pi} \sum_{n=0}^{\infty} \left(\frac{\varepsilon_{on}}{n} \sin \frac{n\pi\Delta X_\ell}{2a} \cos \frac{n\pi X_q}{a} \cos \frac{n\pi X_\ell}{a} \right) T_n'
$$

$$
- \frac{1}{4\pi^2} \left\{ \frac{\Delta Y_\ell}{b} + \xi[1 - \frac{\xi}{b}(Y_q - Y_\ell + \frac{\Delta Y_\ell}{2})] \right.
$$

$$
\left. - \eta[1 - \frac{\eta}{b}(Y_q - Y_\ell - \frac{\Delta Y_\ell}{2})] \right\} \cdot \left\{ \frac{\Delta X_\ell}{a} + \xi' \right.
$$

$$
\left. [1 - \frac{\xi'}{a}(X_q - X_\ell + \frac{\Delta X_\ell}{2})] - \eta'[1 - \frac{\eta'}{a}(X_q - X_\ell - \frac{\Delta X_\ell}{2})] \right\} , \tag{5}
$$

where, for $\left(\frac{n\pi}{a} \right)^2 - k^2 < 0$,

$$
T_n' = \frac{1}{\sinh \alpha'_{11}\pi} \left\{ - \sin \alpha'_{11}\pi [1 - \frac{1}{b}(Y_q + Y_\ell + \frac{\Delta Y_\ell}{2})] \right.
$$

$$
+ \sin \alpha'_{11}\pi[1 - \frac{1}{b}(Y_q + Y_\ell - \frac{\Delta Y_\ell}{2})]
$$

$$
+ \xi \sin \alpha'_{11}\pi[1 - \frac{\xi}{b}(Y_q - Y_\ell + \frac{\Delta Y_\ell}{2})]
$$

$$
\left. - \eta \sin \alpha'_{11}\pi[1 - \frac{\eta}{b}(Y_q - Y_\ell - \frac{\Delta Y_\ell}{2})] \right\} , \tag{6a}
$$

$$
\alpha'_{11} = \frac{b}{\pi} \sqrt{-\left(\frac{n\pi}{a} \right)^2 + k^2} , \tag{6b}
$$

and, for $\left(\frac{n\pi}{a} \right)^2 - k^2 \geq 0$,

10

$$T_n' = \frac{1}{\sinh \alpha_{11}\pi} \left\{ -\sinh \alpha_{11}\pi[1 - \frac{1}{b}(Y_q + Y_\ell + \frac{\Delta Y_\ell}{2})] \right.$$

$$+ \sinh \alpha_{11}\pi[1 - \frac{1}{b}(Y_q + Y_\ell - \frac{\Delta Y_\ell}{2})]$$

$$+ \xi \sinh \alpha_{11}\pi[1 - \frac{\xi}{b}(Y_q - Y_\ell + \frac{\Delta Y_\ell}{2})]$$

$$\left. - \eta \sinh \alpha_{11}\pi[1 - \frac{\eta}{b}(Y_q - Y_\ell - \frac{\Delta Y_\ell}{2})] \right\}, \qquad (7a)$$

and

$$\alpha_{11} = \frac{b}{\pi} \sqrt{\left(\frac{n\pi}{a}\right)^2 - k^2} \quad . \qquad (7b)$$

In Equations (6a) and (7a),

$$\xi = \begin{cases} 1 & \text{for } Y_q - Y_\ell + \frac{\Delta Y_\ell}{2} \geq 0 \\ -1 & \text{otherwise,} \end{cases}, \qquad (8a)$$

and

$$\eta = \begin{cases} 1 & \text{for } Y_q - Y_\ell - \frac{\Delta Y_\ell}{2} \geq 0 \\ -1 & \text{otherwise} \end{cases} \quad . \qquad (8b)$$

Similarly, expressions for $Q_{\ell q}^{22}$ can be obtained by exchanging between m and n, between ΔX_ℓ and ΔY_ℓ, between X_q and Y_q, between X_ℓ and Y_ℓ, and between a and b in Equations (3) through (8). The expressions for $Q_{\ell q}^{33}$ are

$$Q_{\ell q}^{33} = T_{\ell q}^{33} + S_{\ell q}^{33} , \qquad (9)$$

11

where

$$T_{\ell q}^{33} = \frac{j}{2abk^2} \sum_{n=0}^{\infty} \sum_{m=0}^{\infty} \frac{\varepsilon_{on}\varepsilon_{om}}{k_{nm}} \left[\left(\frac{n\pi}{a}\right)^2 + \left(\frac{mr}{a}\right)^2 \right] \frac{4ab}{n\pi m\pi}$$

$$(\sin \frac{n\pi\Delta X_\ell}{2a} \sin \frac{m\pi\Delta Y_\ell}{2b}) \frac{2}{jk_{nm}} \cos[k_{nm}(Z_q - Z_\ell)]$$

$$\exp(jk_{nm} \Delta Z_\ell/2) \sin \frac{n\pi X_q}{a} \sin \frac{n\pi X_\ell}{a} \sin \frac{m\pi Y_q}{b} \sin \frac{m\pi Y_\ell}{b} \qquad (10)$$

$$T_{\ell q}^{33} = T_{a\ell q}^{33} + T_{b\ell q}^{33} \quad . \qquad (11)$$

In Equation (11),

$$T_{a\ell q}^{33} = \frac{1}{4k^2} \left\{ \frac{1}{b}(Y_q + Y_\ell + \frac{\Delta Y_\ell}{2}) - \frac{1}{b}(Y_q + Y_\ell - \frac{\Delta Y_\ell}{2}) \right.$$

$$+ \xi[1 - \frac{\xi}{b}(Y_q - Y_\ell - \frac{\Delta Y_\ell}{2})] - n[1 - \frac{n}{b}(Y_q - Y_\ell - \frac{\Delta Y_\ell}{2})] \right\}$$

$$\cdot \left\{ \frac{1}{a}(X_q + X_\ell + \frac{\Delta X_\ell}{2}) - \frac{1}{a}(X_q + X_\ell - \frac{\Delta X_\ell}{2}) \right.$$

$$+ \xi' [1 - \frac{\xi'}{a}(X_q - X_\ell + \frac{\Delta X_\ell}{2})] - n' [1 - \frac{n'}{a}(X_q - X_\ell - \frac{\Delta X_\ell}{2})] \right\}, \qquad (12)$$

where

$$\xi = \begin{cases} 1 & \text{for } Y_q - Y_\ell + \frac{\Delta Y_\ell}{2} \geq 0 \\ -1 & \text{otherwise} \end{cases},$$

$$n = \begin{cases} 1 & \text{for } Y_q - Y_\ell - \frac{\Delta Y_\ell}{2} \geq 0 \\ -1 & \text{otherwise} \end{cases},$$

$$n' = \begin{cases} 1 & \text{for } X_q - X_\ell - \frac{\Delta X_\ell}{2} \geq 0 \\ -1 & \text{otherwise} \end{cases},$$

$$\xi' = \begin{cases} 1 & \text{for } X_q - X_\ell + \frac{\Delta X_\ell}{2} \geq 0 \\ -1 & \text{otherwise} \end{cases} . \qquad (13)$$

12

Also in Equation (11),

$$S_{b \ell q}^{33} = \frac{-4}{\pi^2} \sum_{n=0}^{\infty} \sum_{m=0}^{\infty} \frac{\epsilon_{on} \epsilon_{om}}{mn\, k_{nm}^2} \sin \frac{n\pi \Delta X_\ell}{2a} \sin \frac{n\pi X_q}{a}$$

$$\sin \frac{n\pi X_\ell}{a} \sin \frac{m\pi \Delta Y_\ell}{2b} \sin \frac{m\pi Y_q}{b} \sin \frac{m\pi Y_\ell}{b} . \qquad (14)$$

It appears that numerical experiments can be fruitfully conducted by letting ΔX_ℓ and ΔY_ℓ vanish as rapidly as ΔZ_ℓ and then observe what correction term $\underline{E}_c(\underline{r})$ should be used. Short of a laboratory experiment, these tests should be very useful in resolving the existing discrepancies in the literature.

It is also interesting to note that a similar singular property has also been observed in Green's function representation of an infinite planar array with wire antenna elements. It was observed that the Green's function has a singular point associated with the component of the equivalent source current in the direction perpendicular to the plane of the array [29, 30]. The computer program yielded good results when the array was made of horizontal dipoles (dipoles parallel to the array plane), but it "blew up" when dealing with vertical dipoles (dipoles perpendicular to the array plane). Since the planar array problem is intimately related to the rectangular waveguide problem, this phenomenon seems to support the result

$$\underline{E}_c = J_z \hat{z} \qquad (15)$$

in References 20, 21, 22 and dispute Yagjian's [18] result which states that

$$\underline{E}_c = \underline{J}/3, \qquad (16)$$

where a cube is chosen as the principal volume.

B. The Temperature Distribution Inside a Biological Body Under Microwave Excitation

The density of power dissipated P_d in a biological body is

$$P_d(\underline{r}) = \omega\varepsilon''(\underline{r}) \; |\underline{E}(\underline{r})|, \tag{17}$$

where ε'' is the imaginary part of the complex permittivity. The density of power dissipated, P_d in Equation (17), can be considered as a distributed heat source inside the biological body. The temperature distribution as a function of time, space, and initial conditions can then be computed from purely thermal considerations. The problem can be formulated by the heat equation [31] as follows

$$\frac{\partial T}{\partial t} = a^2 \; \nabla^2 T + 4\pi a^2 S \; . \tag{18}$$

where T = temperature distribution function,

t = time,

∇^2 = Laplacian operation,

a = $K/\rho c$, K being the heat conductivity, ρ the density, and c the specific heat of the medium,

S = $P_d/4\pi K$, and

P_d = heat source distribution.

Both T and P_d in Equation (18) are functions of time t and spatial coordinate $\underline{r}$. P_d represents the distributed source which is a known quantity computed from Equation (17). The solution of Equation (18) together with all the initial and boundary conditions has been obtained for several elementary geometries [31,32]. For complex geometries, numerical matrix method such as the finite-difference method can be used. For simple cases, an approximate formula used by Guy [23] is very convenient. The short-term temperature rise ΔT is approximately proportional to the power dissipation at the point of interest, namely,

14

$$P_d \approx \iota \, \rho \, c \Delta T, \tag{19}$$

where ρ and c are as defined in Equation (18) and α is a coefficient related to the exposure time. Based on Equation (19), the relative short-time temperature distribution is approximately the same as the density of power dissipation. Guy did not indicate the origin nor the rationale for Equation (19). However, Equation (19) can be considered to be a special case of Equation (18) at a short period after $t = 0$. Since $\nabla^2 T = 0$ at $t = 0-$, as was the usual case, we have $\nabla^2 T \approx 0$ at $T = 0+$, and Equation (18) can be approximated by Equation (19).

Equation (19) is often satisfactory when applied to the interior region of a homogeneous portion of a dielectric body of low thermal conductivity. It fails to provide useful results near the edge of the dielectric body or at the interface of two different types of dielectrics, as was noted by Guy. As shown in Figure 3, Guy's measurement of temperature profile of a block, formed with muscle in Region 1 and fat in Region 2, exhibited gross deviation at the interface from his calculated power dissipation curve. Thus, Equation (19) appeared to fail in the neighborhood of the interface between the fat and the muscle tissues. Guy then proceeded to correct this discrepancy by enforcing the continuity of temperature at the interface. Although his approach appears reasonable on a qualitative basis, many questions remain to be answered.

A more rigorous appraoch was taken in the present study by using the diffusion Equation (18). We first investigated the fat-muscle block of Figure 4, and was able to obtain good numerical results. However, we have found that the temperature distribution is quite time dependent, being fastly varying in the first five seconds. Thus, the temperature profile can not be simply established by recording within, say, five seconds after the heating.

We first examine the case in which the muscle is held at a uniform temperature T_o and the fat is held at $0^\circ k$ at time $t = 0-$ as shown in

15
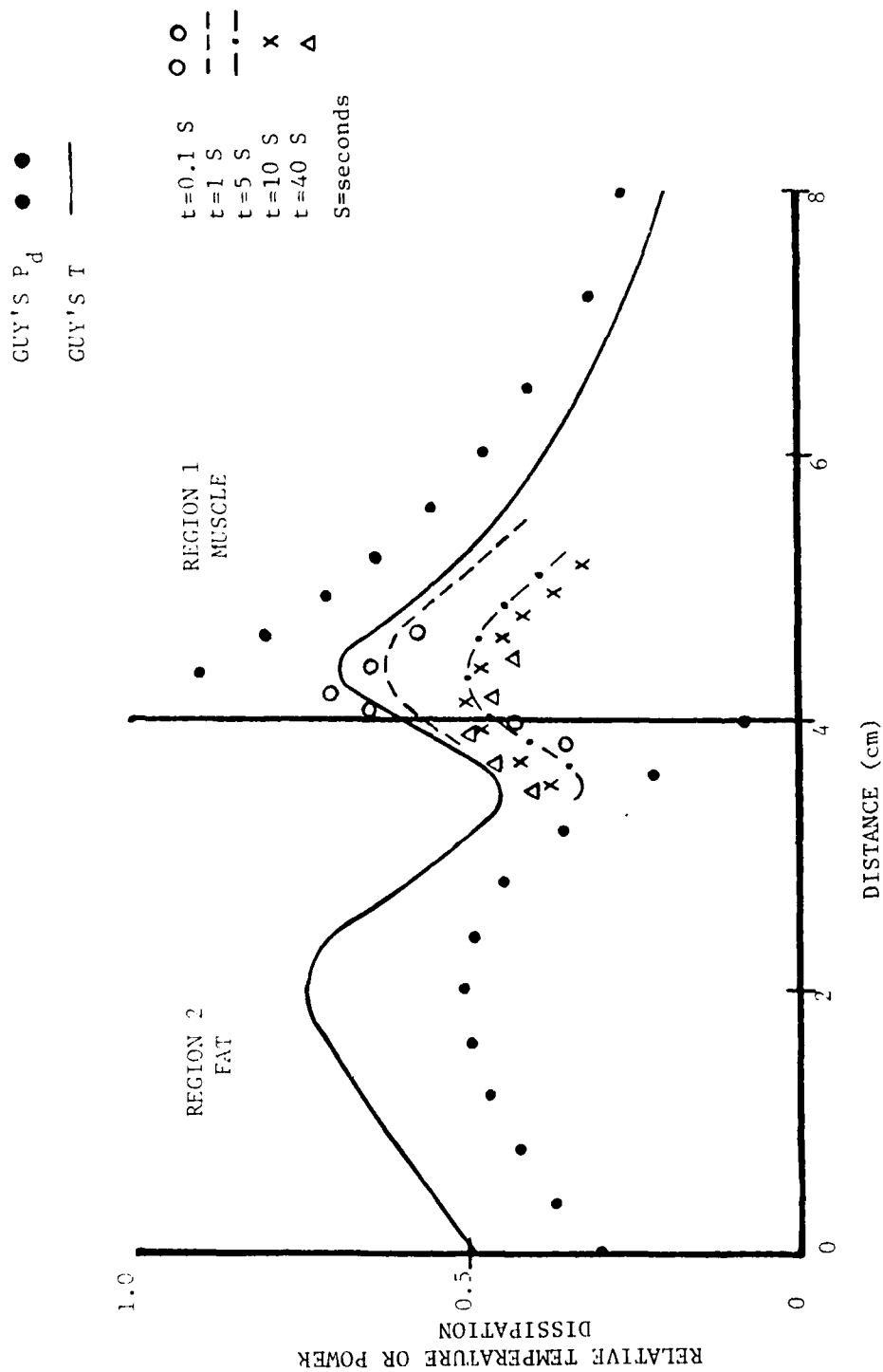
Figure 3. Temperature and power dissipation in the block of fat and muscle studied by Guy.

REGION 1

$T(X,0) = T_o$

K_1, C_1, P_1

MUSCLE

REGION 2

$T(X,0) = 0$

K_2, C_2, P_2

FAT

x

o   a
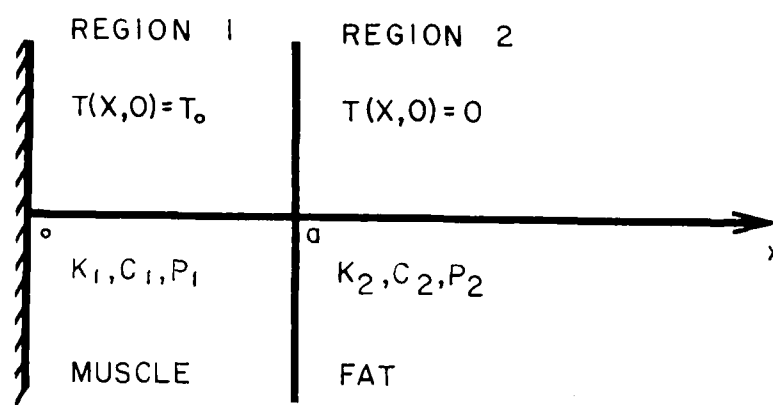
Figure 4.   A one-dimensional composite body of muscle
and fat.

Figure 4.   In the absence of a heating source, the temperature
distribution is [32]

$$T(x,t) = T_o - T_o \frac{1-\beta}{2} \sum_{n=0}^{\infty} \beta^n \left\{ \text{erfc} \; \frac{(2n+1)a - x}{2\sqrt{k_1 t}} \right.$$

$$\left. + \text{erfc} \left[\frac{(2n+1)a + x}{2\sqrt{k_1 t}} \right] \right\} \qquad \text{for } 0 < x < a$$

$$= T_o \frac{1 + \beta}{2} \sum_{n=0}^{\infty} \beta^n \left\{ \text{erfc} \left[\frac{2na + u(x-a)}{2\sqrt{k_1 t}} \right] \right.$$

$$\left. - \text{erfc} \left[\frac{(2n+2)a + u(x-a)}{2\sqrt{k_1 t}} \right] \right\} \qquad \text{for } x > a \qquad (20)$$

where

$$\beta = \frac{K_1 \sqrt{k_2} - K_2 \sqrt{k_1}}{K_1 \sqrt{k_2} + K_2 \sqrt{k_1}} , \qquad (21a)$$

$$k_1 = K_1 / C_1 \quad , \quad \text{and} \qquad (21b)$$

$$k_2 = K_2 / C_2 , \qquad (21c)$$

and k_1, C_1, and k_2, C_2 are the heat conductivity and specific heat for
Regions 1 and 2, respectively.

The temperature profile along the x axis changes rapidly during the
first five seconds, as shown in Figure 5.   As a result, merely recording
the temperature as soon as possible (for example, Guy did it in less
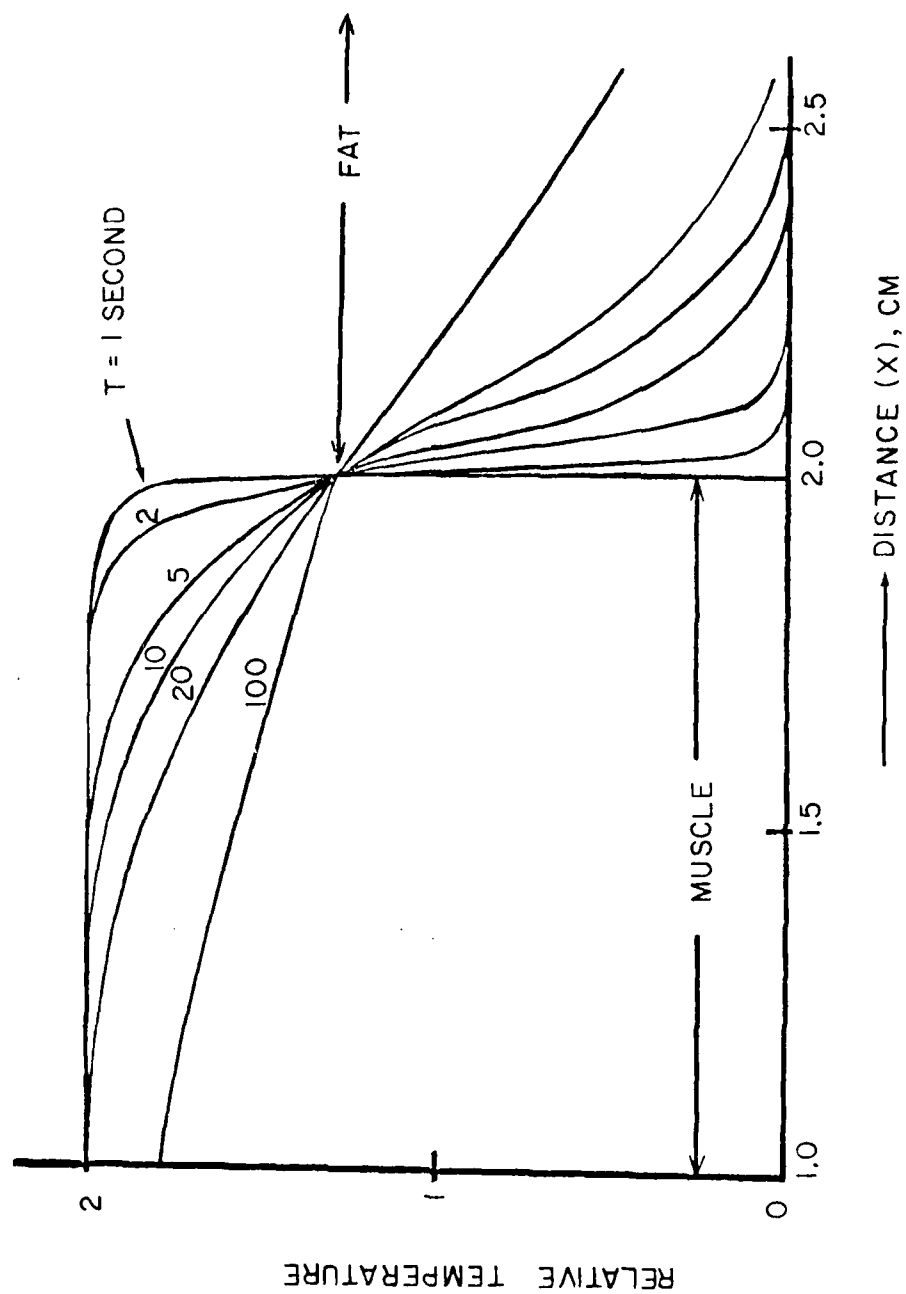than five seconds) does not guarantee consistent and meaningful results.

18

Figure 5. Temperature profile along a composite block of fat and muscle.

Equation (20) can also be employed to compute the approximate temperature for the case in which the initial temperature distribution is not uniform. An example is shown in Figure 3 for the fat-muscle block studied by Guy. The relative temperature distribution can be approximated by modifying the temperature expression of Equation (20) with the nonuniform dissipated power distribution P_d. As can be seen, the temperature peak near the interface on the muscle side shifts along the x axis during the first 10 seconds. This observation is important in understanding the thermographic data obtained in the present research, in which an apparent hot spot near the edge of a tissue has also been observed.

It is difficult to solve Equation (18) for a biological tissue of more complex geometry other than slabs, spheres, ellipsoids, and cylinders. However, it has been observed that the simple approximation of Equation (19) is valid in regions far from sharp temperature gradients such as the edge of or interface in a tissue.

SECTION III

COMPARISON WITH THERMOGRAPHIC MEASUREMENTS

Two types of thermographic measurements were made: one using thermographic paper and the other using thermographic camera. The thermograhic paper measures the peak temperature during and after the exposure time but does not record accurate data. Furthermore, it is always difficult to place a thermographic paper at the proper location without affecting the experiment. The thermographic camera is more accurate but is also difficult to look at the inside of a tissue. As has been discussed in the preceding section, the temperature distribution varies with time. Merely taking a quick picture immediately after heat exposure does not always yield consistent data. Consequently, great care must be taken when comparing the calculated and measured thermal data. Measurements were made at WRAIR, even though some preliminary tests were performed at Georgia Tech. All the cases studied were rectangular-sided blocks which are convenient for the book-keeping of the location of the field points.

Figure 6 shows a comparison between the calculated dissipated power intensity and the temperature profile recorded with thermographic paper for Case C in Reference 13. Although a general agreement can be observed in the comparison, the thermographic measurement was difficult to calibrate and repeat. The dielectric model used had a high water content which generated hot steam during the later stage of the exposure. A power level of 15 to 50 watts was used, and exposure times of 15 to 25 minutes were tried. Usually four or more recordings of different exposure times must be tried before a recording of good quality can be obtained.

Figure 7 shows the physical configuration of a dielectric (Stycast Hi-K16) block inside a WR284 waveguide. The block is divided into 54 identical cells which were numbered as shown in the figure. The calculated dissipated power intensity at the center of each cell on the top layer is plotted in Figure 8 in a perceptive view. Two temperature profiles measured with a heat-sensitive camera are shown in

21

(b) 2.65 GHz
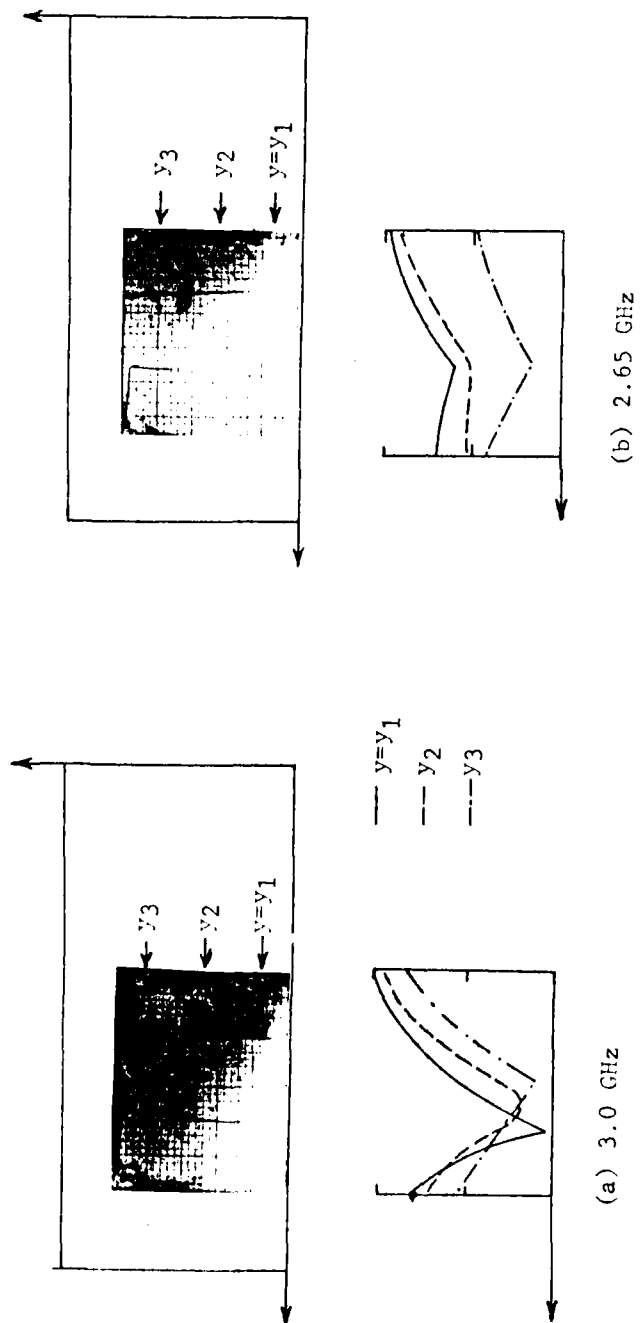
(a) 3.0 GHz

y=y₁
y₂
y₃

Figure 6. Calculated distribution of dissipated power in comparison with thermographic measurements.
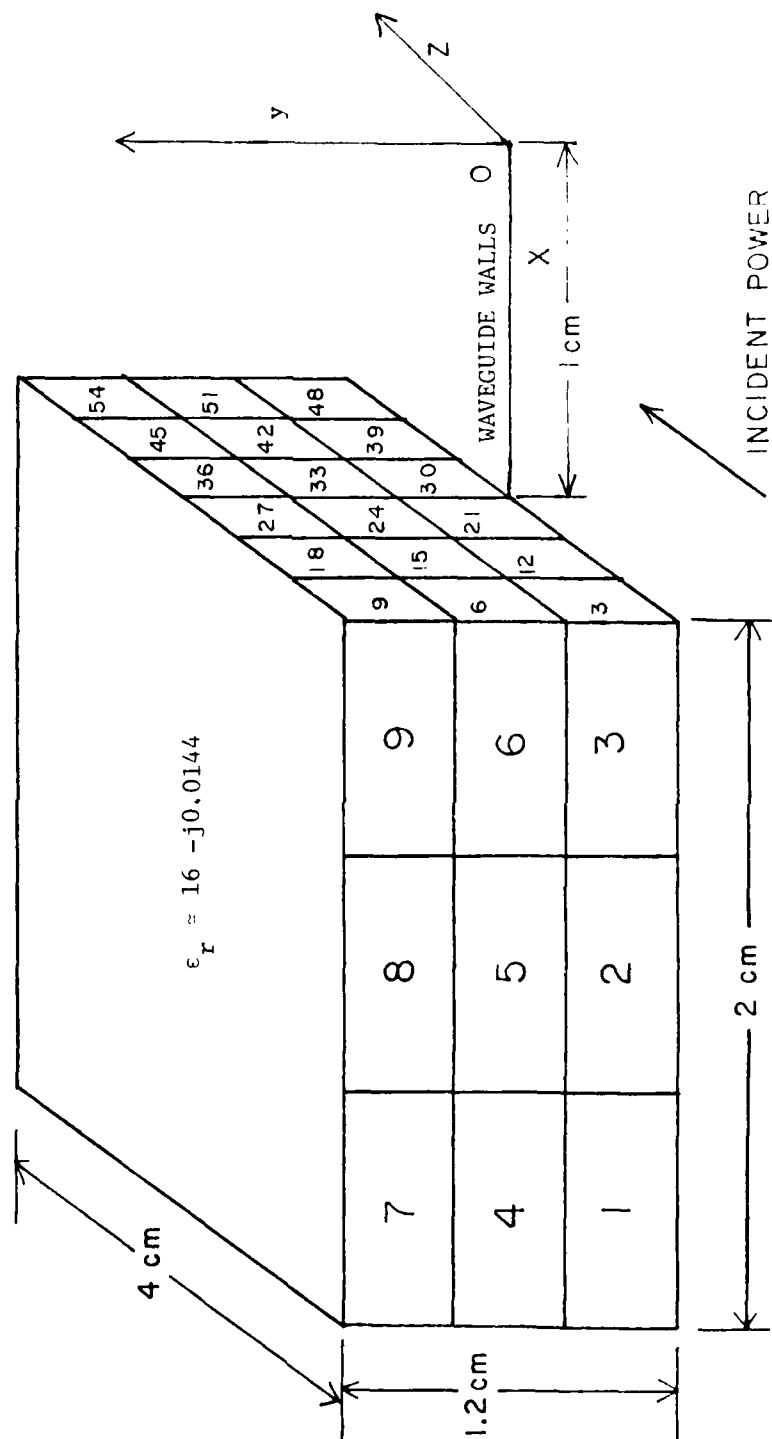
22

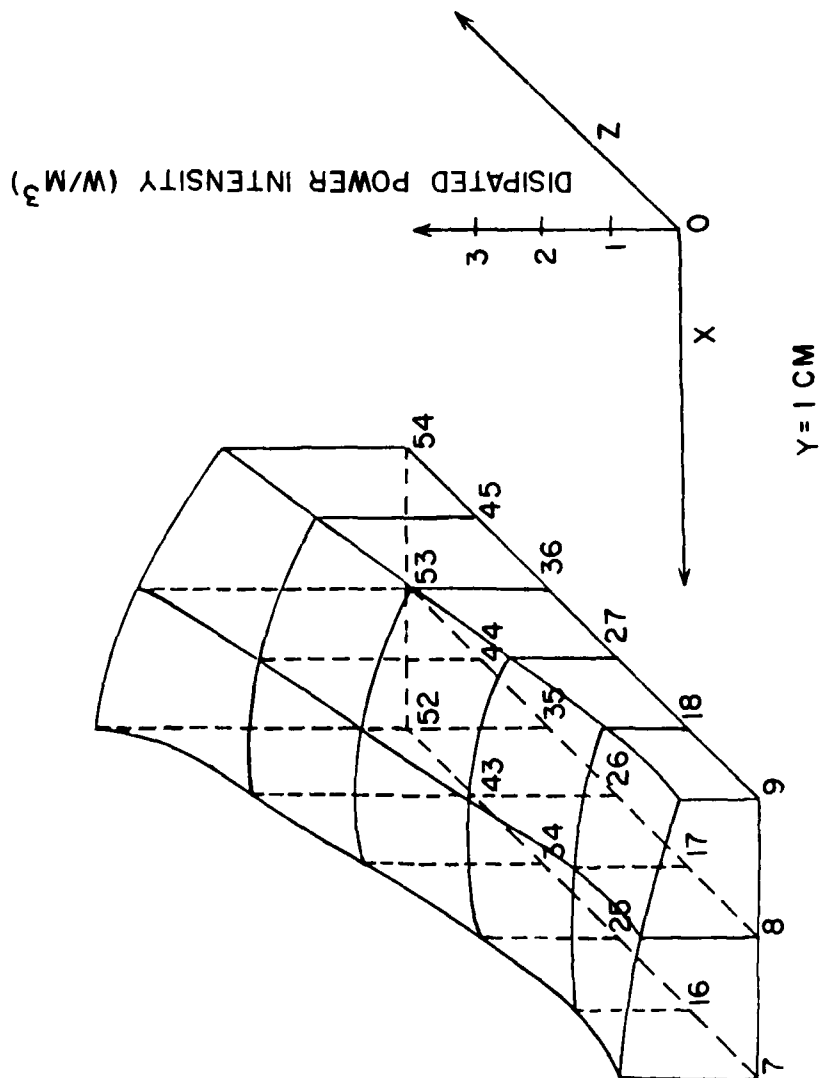Figure 7. A dielectric block inside a rectangular WR284 waveguide.

Figure 8. Distribution of dissipated power intensity over a plane passing through the center of the top layer of the block in Figure 7.

Figure 9 for comparison. Satisfactory agreement is observed except for a discrepancy on the far end of the block where the calculated power dissipation continuously rises toward the edge of the block while the measured temperature shows a drop near the edge. This disagreement can be explained in the following manner.

As has been discussed in the preceding section, the temperature distribution is approximately proportional to the dissipated power intensity only for a brief period after the exposure and only for regions away from the surfaces with discontinuity of thermal coefficients. The drop-off of the temperature near the distal (load) end of the block can be explained in the same manner it was in Figures 3 and 5. The calculated power dissipation corresponding to (a) of Figure 9 is plotted in Figure 10 in the same fashion. Good numerical convergence is indicated in computations using 24, 54, and 63 cells. The 63-cell calculation employed a configuration of unequal cell volumes to obtain great details in the questioned distal end near $z = 2$ cm. As can be seen, there is a definite rise in power dissipation toward the edge of the block. Temperature distribution is calculated using thermal conductivities of 0.0084 and 0.0008 watts/cm-°K for specific heats of 4.186 and 0.1 joules/cm^3-°K for the dielectric and the air, respectively. The resulting temperature fall-off, however, was much closer to the edge than the measured data in Figure 9(a). We have found, however, that the temperature peak can be shifted away by as much as 0.4 cm from the edge by using different thermal coefficients in the computation. Therefore, the calculation could be improved by using more reliable thermal coefficients and by a more refined thermal modeling approach.

(a) Along the waveguide axis

y = 1.2 cm

x = 3 cm
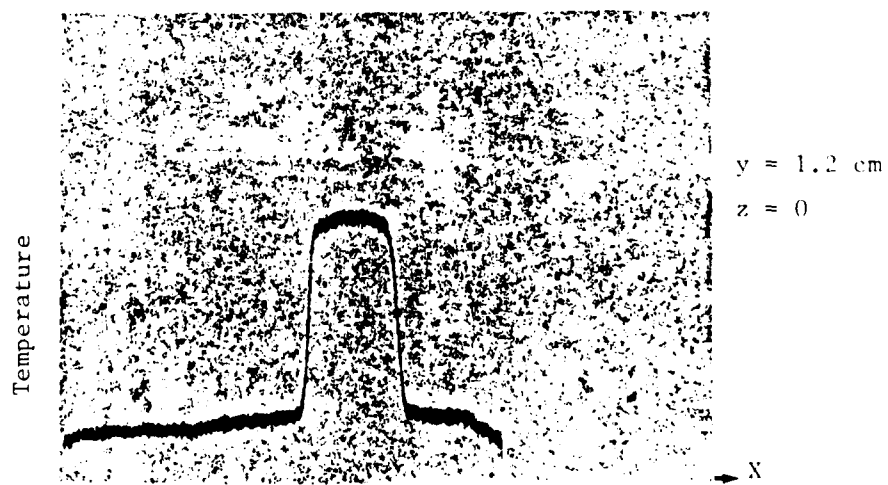
(b) Perpendicular to the waveguide axis

y = 1.2 cm

z = 0

Figure 9.   Thermographic measurements on the top surface of the block sample of Figure 7.
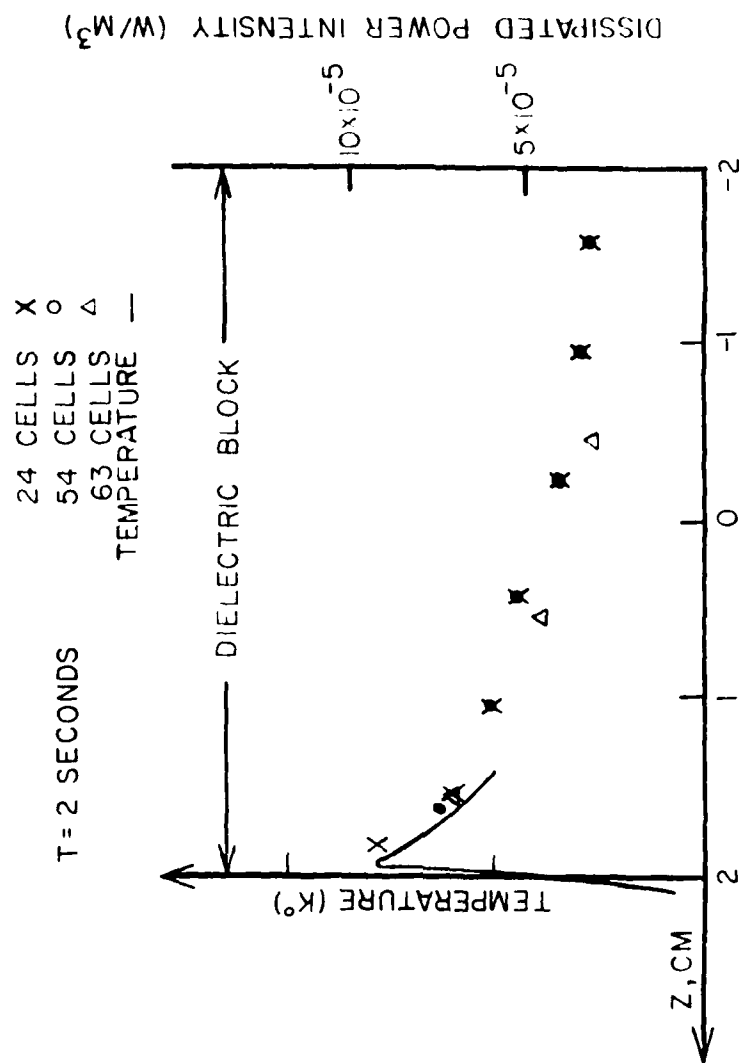
Figure 10. Calculated dissipated power intensity and temperature for comparison with the measured results of Figure 9(a).

27

SECTION IV
CONCLUSIONS AND RECOMMENDATIONS

An analytical tool has been developed to compute the electromagnetic fields inside a three-dimensional arbitrarily-shaped heterogeneous dielectric or biological body inside a rectangular waveguide. The profile of dissipated power intensity, and hence the temperature, can be determined with satisfactory accuracy. Immediate application of this technique will be to provide guidance for the design of microwave applicators for rapid inactivation of enzymes. The techniques involved in the present analysis represent advances in microwave and electromagnetic theory. Their impact could be extended into other physical and mathematical sciences.

Numerical tests have been conducted for rectangular-sided homogeneous bodies only, even though the computer program was written for a general three-dimensional arbitrarily-shaped heterogeneous body. The computer program was checked by numerical convergence tests and conservation of energy, as well as by direct comparison with measured reflection and thermographic data. For dielectric bodies of low to medium dielectric constants (less than, say, 15), excellent results were obtained. The quality of the results degraded gradually with increasing dielectric constants. However, even for high dielectric constants of about 50, fairly good results were yielded by the computer program.

Further research should include test cases of biological bodies of greater complexity, such as a two layer ellipsoid or even a full rat configuration. In addition, the waveguide structure can be modified to represent a more practical applicator such as a waveguide with a shorting plate at the end. These tasks have been initiated during the present grant period but could not be completed with the limited funds available.

It is also recommended that a more accurate theoretical approach be established to relate the distributed power dissipation and the temperature profile inside the biological body. Extensive numerical

data should be generated to guide the applicator design. However,
improvements of the existing algorithm must be made before data
generation, since the computer runs are quite costly.

SECTION V

REFERENCES

1. E.W. Sutherland and T.W. Rall, "Relation of Adenosine – 3', 5'-Phosphate and Phosphorylase to the Actions of Catecholamines and Other Hormones," Pharm. Rev., Vol. 12, p. 265, 1960.

2. R.W. Butcher, G.A. Robison, J.G. Hardman, and E.W. Sutherland, "The Role of Cyclic AMP in Hormone Actions," Advan. Enzyme Regul., Vol. 6, p. 357, 1968.

3. B. Breckenridge, "Cyclic AMP and Drug Action," Ann. Rev. Pharmacol., Vol. 10, p. 19, 1970.

4. G.R. Siggins, B.J. Hoffer, and F.E. Bloom, "Cyclic Adenosine Monophosphate: Possible Mediator for Norepinephrine Effects on Cerebellar Purkinje Cells," Science, Vol. 165, p. 1018, 1969.

5. D.A. McAfee, M. Schorderet, and P. Greengard, "Adenosine 3', 5'-Monophosphate in Nervous Tissue: Increase Associated With Synaptic Transmission," Science, Vol. 171, p. 1156, 1971.

6. B. Breckenridge, "The Measurement of Cyclic Adenylate in Tissues," Proc. Nat. Acad. Sci., Vol. 52, p. 1580, 1964.

7. O. Lowrey, J. Passonneau, F. Hasselberger, and D. Schutz, "Effect of Ischemia on Known Substrates and Cofactors of the Glycolytic Pathway in Brain," J. Biol. Chem., Vol. 239, p. 18, 1964.

8. W.B. Stavinoha, B. Pepeko, and P. Smith, "The Use of Microwave Heating in Inactivate Cholinesterase in the Rat Brain Prior to Analysis for Acetylcholine," Parmacologist, Vol. 12, p. 257, 1970.

9. D.F. Swaab, "Pitfalls in the Use of Rapid Freezing for Stopping Brain and Spinal Cord Metabolism in Rat and Mouse," J. Neurochem., Vol. 20, pp. 183-188, 1973.

10. R.L. Veech, R.L. Harris, D. Veloso, and E.H. Veech, "Freeze-Blowing: A New Technique of the Study of Brain In-Vivo," J. Neurochem., Vol. 20, pp. 183-188, 1973.

11. E.W. Sutherland and T.W. Rall, "Fractionation and Characterization of a Cyclic Adenine Ribonucleotide Formed by Tissue Particles," J. Biol. Chem., Vol. 232, p. 1077, 1958.

12. R.H. Lenox, O.P. Gandhi, J.L. Meyerhoff, and H.M. Grove, "A Microwave Applicator for In-Vivo Rapid Inactivation of Enyzmes in the Central Nervous System," IEEE Trans. on Microwave Theo. Tech., Vol. MTT-24, No. 1, pp. 58-61, January 1978.

13. J.J.H. Wang, "Analysis of a Three-Dimensional Arbitrarily-Shaped Dielectric or Biological Body Inside a Rectangular Waveguide," IEEE Trans. on Microwave Theo. Tech., Vol. MTT-26, No. 7, pp. 457-462, July 1978 (see Appendix).

14. P. Silvester and Z.J. Csendes, "Numerical Modeling of Passive Microwave Devices," IEEE Trans. Microwave Theo. Tech., Vol. MTT-22, pp. 190-201, March 1974.

15. R.L. Ferrari and G.L. Maile, "Three-Dimensional Finite-Element Method for Solving Electromagnetic Problems," Electronics Letters, Vol. 14, No. 15, pp. 467-468, July 1978.

16. S. Akhtarzad and P.B. Johns, "Three-Dimensional Transmission-Line Matrix Computer Analysis of Microstrip Resonators," IEEE Trans. Microwave Theo. Tech., Vol. MTT-23, No. 12, pp. 990-997, December 1975.

17. A.D. Yaghjian, "A Direct Approach to the Derivation of Electric Dyadic Green's Functions," Digest of 1976 IEEE International Symposium on Antennas and Propagation, Amherst, MA., pp. 71-73, October 1976.

18. A.D. Yagjian, "A Direct Approach to the Derivation of Electric Dyadic Green's Functions," NBS Technical Note 1000, January 1978.

19. C.T. Tai, Dyadic Green's Functions in Electromagnetic Theory, Scranton, PA., Intext Educational Publishers, 1972.

20. C.T. Tai, "On the Eigen Function Expansion of Dyadic Green's Functions," Proc. of IEEE, Vol. 61, p. 480, April 1973.

21. Y. Rahmat-Samii, "On the Question of Computation of the Dyadic Green's Function at the Source Region in Waveguides and Cavities," IEEE Trans. Microwave Theo. Tech., Vol. MTT-23, pp. 762-765, September 1975.

22. R.E. Collin, "On the Incompleteness of E- and H- Modes in Waveguides," Can. J. Phys., Vol. 51, pp. 1135-1140, 1973.

23. A.W. Guy, "Analysis of Electromagnetic Fields Induced in Biological Tissues by Thermographic Studies on Equivalent Phantom Models," IEEE Trans. Microwave Theo. Tech., Vol. MTT-19, No. 2, pp. 205-214, February 1971.

24. A.W. Guy, "Physical Aspects of the Electromagnetic Heating of Tissue Volume," International Symposium on Cancer Therapy by Hyperthermia and Radiation, Washington, D.C. pp. 179-192, April 1975.

25. K.M. Chen, "A Simple Physical Picture of Tensor Green's Function in Source Region," Proc. IEEE., Vol. 65, pp. 1202-1204, August 1977.

26. O.D. Kellogg, Foundations of Potential Theory, Springer-Verlag, Berlin, Germany, 1929.

27. J. Van Bladel, "Some Remarks on Green's Dyadic for Infinite Space," IRE Trans. Antennas and Propagation, Vol. AP-9, pp. 563-566, November 1961.

31

28. J.J.H. Wang, F.L. Cain, and E.C. Burdette, "Numerical Modeling of Three-Dimensional Arbitrarily-Shaped Heterogeneous Biological Bodies Under Complex Excitations," Digest of 1978 Symposium on Electromagnetic Fields in Biological Systems, Ottawa, Canada, June 1978.

29. J.A. Fuller and R.L. Moore, "Hardened Phased-Array Feasibility Assessment," Technical Report on Project A-1863, Contract No. DASG60-76-C-0070, Engineering Experiment Station, Georgia Institute of Technology, Atlanta, GA., July 1977.

30. J.J.H. Wang, "Status and Recommendations on the Array Analysis of A-1863," Internal Memorandum, Project A-1863, Engineering Experiment Station, Georgia Institute of Technology, November 1977.

31. P.M. Moore and H. Feshback, Methods of Theoretical Physics, New York: McGraw-Hill Co., 1953.

32. R.V. Churchill, Operational Mathematics, New York: McGraw-Hill Co., 1958.

APPENDIX

REFERENCE 13

Analysis of a Three-Dimensional Arbitrarily Shaped Dielectric or Biological Body Inside a Rectangular Waveguide

JOHNSON J. H. WANG, MEMBER, IEEE

Abstract—This paper presents a method for the analysis of three-dimensional arbitrarily shaped dielectric obstacles inside a rectangular waveguide. The numerical computation involves a dyadic Green's function containing a double infinite series, which is evaluated by a partial summation technique.

I. Introduction

WAVEGUIDE obstacles and discontinuities, including the dielectric type to be discussed in this paper, are long standing problems in electromagnetic theory. Many of them, essentially two dimensional, have been solved and were summarized by Marcuvitz [1]. The general three-dimensional discontinuity problems, however, remain unsolved in spite of the advent of modern high-speed digital computers and the method of moments [2] which permit treatment of problems not solvable by exact methods. Upon reviewing the status of numerical techniques for passive microwave devices, Silvester and Csendes [3] observed in 1974, "not a single truly three-dimensional solution has been published" for waveguide discontinuity problems. This statement is apparently still valid today.

This lack of published research activities in three-dimensional waveguide discontinuities has been in many circumstances due to the deficiencies of the Green's functions in the waveguide region. A dyadic Green's function for the rectangular waveguide was presented by Tai in 1972 [4] and later revised by the same author in 1973 [5]. Tai's expression includes a double infinite series summing over the contributions from all the individual waveguide modes. Recalling the simple expression of the free space Green's function, one immediately recognizes the greater complexity in the waveguide case.

This paper presents a successful use of the dyadic Green's function in the analysis of the electromagnetic problem of a three-dimensional arbitrarily shaped dielectric or biological body inside a rectangular waveguide. In the process, the extremely slow convergence of the double infinite series in the Green's function had to be modified by means of a partial summation technique. The immediate application of this new analytical technique is in
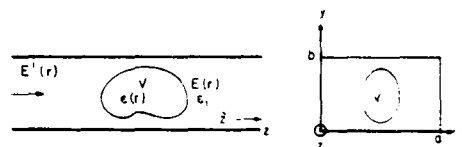
Fig. 1. A three-dimensional arbitrarily shaped heterogeneous dielectric body illuminated inside a rectangular waveguide.

microwave waveguide enzyme inactivation in neuro-chemical research [6]. Extension of this technique to highly conductive obstacles is feasible but may require modification of the volume integral into a surface expression.

II. The Integral Equation and the Dyadic Green's Function

The problem to be considered is shown in Fig. 1, in which a three-dimensional arbitrarily shaped heterogeneous dielectric or biological body is electromagnetically illuminated in a rectangular waveguide. The dielectric body has a permittivity distribution of $\epsilon(r)$, where r is a positional vector. Outside the volume V occupied by the dielectric body, the permittivity is homogeneous and is denoted by ϵ_1. Free space permeability μ_0 is assumed for both the dielectric body and the medium outside V.

The time function $e^{-j\omega t}$, where t and ω are time and radian frequency, is used in all the equations in this paper for ready comparison with Tai's work [4], [5]. Since the $e^{j\omega t}$ convention is perhaps more widely used, a comment on the conversion of the equations to this convention is justified at this point. For the $e^{j\omega t}$ convention, one merely changes to $-j$ all the j's appearing in the equations in this paper.

In Fig. 1, $E(r)$ denotes the electric field intensity at r and $E'(r)$ denotes the field intensity at r with the dielectric body replaced by the medium ϵ_1. The scattered field is defined as

$$E^s(r) = E(r) - E'(r). \qquad (1)$$

The volume equivalence principle can be shown to be valid in the bounded as well as the unbounded space. As a result, the problem as depicted in Fig. 1 is equivalent everywhere to a homogeneous waveguide with ϵ_1, μ_0, and with volume current density

$$J(r) = -j\omega \left[\epsilon(r) - \epsilon_1 \right] E(r). \qquad (2)$$

It follows from the theorem of superposition that the electric field radiated from $J(r)$ is equal to $E^s(r)$. Therefore,

$$E^s(r) = j\omega\mu_0 \int_V \bar{G}_e(r,r') \cdot J(r') \, dV' \tag{3}$$

where $\bar{G}_e$ is the dyadic Green's function of the electric type and

$$\bar{G}_e(r,r') = \bar{G}_{e0}(r,r') - \frac{1}{k_1^2} \hat{z}\hat{z}\,\delta(r,r') \tag{4}$$

where δ denotes a three-dimensional Dirac delta function, $\hat{z}$ denotes a unit vector along z, $k_1 = \omega\sqrt{\epsilon_1\mu_0}$, and $\bar{G}_{e0}$ is defined below. The term involving δ had not been included in Tai's earlier work [4] until 1973 [5] and has been a subject of recent discussions [5], [7], [8]. $\bar{G}_{e0}$ was not explicitly expressed in the literature except by Rahmat-Samii [7]. However, Rahmat-Samii's expression has a number of errors in the print. For the clarity of the present discussion and the convenience of future references, it is desirable to present it in the following long form:

$$\bar{G}_{e0}(r,r') = \frac{j}{2abk_1^2} \sum_{m=0}^{\infty} \sum_{n=0}^{\infty} \frac{\epsilon_{0n}\epsilon_{0m}}{k_{mn}} e^{jk_{mn}|z-z'|}$$

$$\cdot \left\{ \hat{x}\hat{x}\left[k_1^2 - \left(\frac{m\pi}{a}\right)^2 \right] \cos\frac{m\pi x}{a} \cos\frac{m\pi x'}{a} \right.$$

$$\cdot \sin\frac{n\pi y}{b} \sin\frac{n\pi y'}{b} + \hat{y}\hat{y}\left[k_1^2 - \left(\frac{n\pi}{b}\right)^2 \right] \sin\frac{m\pi x}{a} \sin\frac{m\pi x'}{a}$$

$$\cdot \cos\frac{n\pi y}{b} \cos\frac{n\pi y'}{b} + \hat{z}\hat{z}\left[\left(\frac{m\pi}{a}\right)^2 + \left(\frac{n\pi}{b}\right)^2 \right]$$

$$\cdot \sin\frac{m\pi x}{a} \sin\frac{m\pi x'}{a}$$

$$\cdot \sin\frac{n\pi y}{b} \sin\frac{n\pi y'}{b} + \hat{x}\hat{y}\left[-\left(\frac{m\pi}{a}\right)\cdot\left(\frac{n\pi}{b}\right) \right]$$

$$\cdot \cos\frac{m\pi x}{a} \sin\frac{m\pi x'}{a}$$

$$\cdot \sin\frac{n\pi y}{b} \cos\frac{n\pi y'}{b} + \hat{y}\hat{x}\left[-\left(\frac{m\pi}{a}\right)\cdot\left(\frac{n\pi}{b}\right) \right]$$

$$\cdot \sin\frac{m\pi x}{a} \cos\frac{m\pi x'}{a}$$

$$\cdot \cos\frac{n\pi y}{b} \sin\frac{n\pi y'}{b} + \hat{y}\hat{z}\left[\pm jk_{mn}\frac{n\pi}{b} \right] \sin\frac{m\pi x}{a} \sin\frac{m\pi x'}{a}$$

$$\cdot \cos\frac{n\pi y}{b} \sin\frac{n\pi y'}{b} + \hat{z}\hat{y}\left[\mp jk_{mn}\frac{n\pi}{b} \right] \sin\frac{m\pi x}{a} \sin\frac{m\pi x'}{a}$$

$$\cdot \sin\frac{n\pi y}{b} \cos\frac{n\pi y'}{b} + \hat{z}\hat{x}\left[\mp jk_{mn}\frac{m\pi}{a} \right] \sin\frac{m\pi x}{a} \cos\frac{m\pi x'}{a}$$

$$\cdot \sin\frac{n\pi y}{b} \sin\frac{n\pi y'}{b} + \hat{x}\hat{z}\left[\pm jk_{mn}\frac{m\pi}{a} \right] \cos\frac{m\pi x}{a} \sin\frac{m\pi x'}{a}$$

$$\left. \cdot \sin\frac{n\pi y}{b} \sin\frac{n\pi y'}{b} \right\}, \quad \text{for } z \gtrless z' \tag{5}$$

where

$$\epsilon_{0n} = \begin{cases} 1, & \text{if } n = 0 \\ 2, & \text{otherwise} \end{cases}$$

$r = $ field point $= (x,y,z)$

$r' = $ source point $= (x',y',z')$

$$k_{mn} = \begin{cases} |(k_1^2 - k_c^2)^{1/2}|, & \text{if } k_{mn} \text{ is real} \\ j|(k_c^2 - k_1^2)^{1/2}|, & \text{if } k_{mn} \text{ is imaginary} \end{cases}$$

where

$$k_c^2 = \left(\frac{m\pi}{a}\right)^2 + \left(\frac{n\pi}{b}\right)^2.$$

Equations (1)–(4) can be manipulated to yield the following integral equation:

$$j\omega\mu_0 \int_V \bar{G}_{e0}(r,r') \cdot J(r) \, dV' + \frac{J(r)}{j\omega[\epsilon(r) - \epsilon_1]}$$

$$+ \frac{J_z(r)\hat{z}}{j\omega\epsilon(r)} = -E(r) \tag{6}$$

where J_z is the z component of J. The unknown J in (6) can then be solved by the method of moments [2] which transforms the integral equation into a set of linear equations readily solvable by means of a digital computer.

III. Solution by the Method of Moments

Although there exists a number of methods by which an integral equation can be solved numerically, the complexity of three-dimensional geometry can hardly tolerate further complication in the computational process. Even in the much simpler case of plane wave incidence and unbounded free space, only point matching together with rectangularly sided cells has been attempted for the volume type of integral equation [9]. Fortunately, this unsophisticated process has been found to be capable of producing good numerical results. Thus point matching with rectangularly sided cells is employed in the present analysis.

The volume V occupied by the dielectric body is first divided into L equal rectangular-sided cells $\Delta V_1 - \Delta V_L$, each of which has constant dimensions Δx, Δy, and Δz. The electric field, assumed to be uniform inside the lth cell, is designated as $E(r_l)$, where r_l represents the center of the lth cell. The equivalent current in (2) can then be expressed as

$$J(r) = \sum_{l=1}^{L} \sum_{k=1}^{3} J_l^k B_l^k(r) \tag{7}$$

where B_l^k is a basis function defined as

$$B_l^k(r) = \hat{u}_k P^l(r), \qquad k = 1,2,3 \text{ or } x,y,z \tag{8}$$

$\hat{u}_k$ in (8) denotes a unit vector, and

$$P^l(r) = \begin{cases} 1, & \text{for } r \text{ in } \Delta V_l \\ 0, & \text{elsewhere.} \end{cases} \tag{9}$$

The weighting function is defined as

$$W_q^p(r) = \delta(r - r_q)\hat{u}_p, \qquad p = 1, 2, 3. \qquad (10)$$

The scalar product between f and g is defined as

$$(f, g) = \int_V f \cdot g \, dv. \qquad (11)$$

We can generate a set of linear equations by first substituting (7) into (6) and then performing a scalar product on the resulting equation with the weighting function of (10) for $p = 1, 2, 3$ and $q = 1, \cdots, L$. This moment generating procedure leads to the following set of equations:

$$\sum_{k=1}^{3} \sum_{l=1}^{L} J_l^k A_{kl}^{pq} = C^{pq}, \qquad p = 1, 2, 3; \, q = 1, \cdots, L \qquad (12)$$

where

$$C^{pq} = -E^i(r_q) \qquad (13)$$

$$A_{kl}^{pq} = j\omega\mu_0 Q_{lq}^{pk} + \frac{\delta_q^l}{j\omega} \left[\frac{\delta_k^p}{\epsilon(r_q) - \epsilon_1} + \frac{\delta_3^k \cdot \delta_3^p}{\epsilon(r_q)} \right]. \qquad (14)$$

δ_k^p in (14) is the Kronecker delta, being 1 when $p = q$ and 0 otherwise, and

$$Q_{lq}^{pk} = \int_{\Delta V_l} G_{e0}^{pk}(r_q, r') \, dV' \qquad (15)$$

where G_{e0}^{pk} is the (p, k) component of the dyad $\bar{G}_{e0}$. The integration in (15) can be carried out to yield

$$Q_{lq}^{pk} = \frac{j}{2abk^2} \sum_{n=0}^{\infty} \sum_{m=0}^{\infty} \frac{\epsilon_{0n}\epsilon_{0m}}{k_{mn}} IQF_{mn}^{pk} \qquad (16)$$

where

$$F_{mn}^{pk} = \left[\text{the } (m, n)\text{th term of } G_{e0}^{pk} \right] \cdot e^{-jk_{mn}|z_q - z_l|} \qquad (17)$$

$$Q = \frac{4ab}{n\pi m\pi} \sin \frac{n\pi \Delta X_l}{2a} \sin \frac{m\pi \Delta Y_l}{2b} \qquad (18)$$

and I in (16) depends on the index pk. For pk being (1,3), (2,3), (3,1), (3,2), where (1,2,3) corresponds to (x, y, z), we have

$$I = \begin{cases} \pm \dfrac{2}{k_{mn}} e^{jk_{mn}|z_q - z_l|} \sin \left(k_{mn} \dfrac{\Delta z_l}{2} \right), & \text{if } z_q \gtrless z_l + \dfrac{\Delta z_l}{2} \\[2mm] \dfrac{2}{k_{mn}} e^{jk_{mn}\Delta z_l/2} \sin \left[k_{mn}(z_q - z_l) \right], & \text{otherwise.} \end{cases} \qquad (19)$$

For other pk indices, we have

$$I = \begin{cases} \dfrac{2}{jk_{mn}} \left\{ \cos \left[k_{mn}(z_q - z) \right] e^{jk_{mn}\Delta z_l/2} - 1 \right\}, \\[1mm] \qquad\qquad \text{if } z_l + \dfrac{\Delta z_l}{2} > z_q > z_l - \dfrac{\Delta z_l}{2} \\[2mm] \dfrac{2}{k_{mn}} \sin \left(k_{mn} \dfrac{\Delta z_l}{2} \right) e^{jk_{mn}|z_q - z_l|}, \qquad \text{otherwise.} \end{cases} \qquad (20)$$
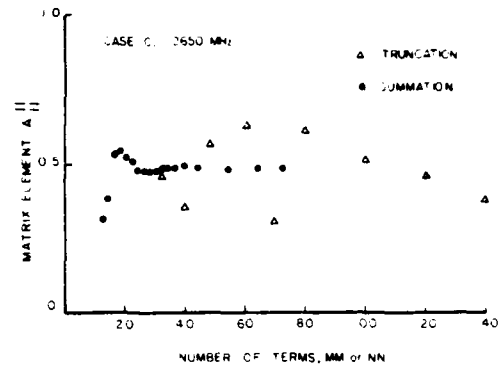

Fig. 2. Comparison of convergence between direct truncation and partial summation.

As can be seen in (14)–(20), the matrix element A_{kl}^{pq} involves a double infinite series which does not converge rapidly unless $|z_q - z_l|$ is large. When $p = q$ as is the case for the self cells which are the diagonal matrix elements $|z_q - z_l| = 0$ and the series convergence is extremely slow. As an example, Fig. 2 shows that no sign of convergence is exhibited even after 140×140 terms are used in the summation. Thus the computation of the matrices can not be carried out by a simple truncation of the series.

This computational difficulty can be surmounted by direct summation of the part of the infinite series which contains terms nonvanishing with increasing M and N. This partial summation transforms a matrix element of a double infinite series into a single infinite series or even into an expression of closed form, which can be truncated for computation. Fig. 2 shows that convergence is achieved with about 20×20 terms for the partial-summation technique, which is significant improvement over the direct truncation method. For most off-diagonal matrix elements, direct truncation is satisfactory because of the predominant influence of the exponential terms with the argument of $jk_{mn}|z_q - z_l|$ or $jk_{mn}\Delta z_l/2$ as shown in (19) and (20). As a result of these exponential terms which rapidly decrease with m and n, off-diagonal matrices with nonvanishing $|z_l - z_q|$ can be computed with a finite series truncated according to a precision criterion established by the value of $jk_{mn}|z_q - z_l|$. Depending on the value of $|z_q - z_l|$, approximately 16×8 up to 21×12 terms were used for m and n in the examples reported in this paper.

The partial summation technique is tedious but straightforward. The portion of the infinite series which consists of terms slowly convergent with m and n are summed by means of the following formulas [10]:

$$\sum_{k=1}^{\infty} \frac{\sin kx}{k} = \frac{\pi - x}{2}, \qquad [0 < x < 2\pi]$$

$$\sum_{k=1}^{\infty} \frac{k \sin ka}{k^2 + a^2} = \frac{\pi}{2} \frac{\sin ha(\pi - x)}{\sin ha\pi}, \qquad a^2 > 0, \, 0 < x < 2\pi$$

$$\sum_{k=0}^{\infty} \frac{k \sin kx}{k^2 - a^2} = \pi \frac{\sin \left\{ a\left[(2m+1)\pi - x \right] \right\}}{2 \sin a\pi},$$

$$2m\pi \leqslant x \leqslant (2m+2)\pi, \qquad a \text{ being noninteger}$$

$$\sum_{k=1}^{\infty} \frac{\cos kx}{k^2 + a^2} = \frac{\pi}{2a} \frac{\cos h(\pi - x)}{\sin ha\pi} - \frac{1}{2a^2}, \qquad 0 < x \leqslant 2\pi$$

$$\sum_{k=1}^{\infty} \frac{\cos kx}{k^2 - a^2} = \frac{1}{2a^2} - \frac{\pi}{2} \frac{\cos a\left[(2m+1)\pi - x\right]}{a \sin a\pi},$$

$$2m\pi \leqslant x \leqslant (2m+2)\pi, \qquad a \text{ being noninteger}.$$

The explicit expressions for the matrix elements after partial summation are too complex to be presented in this paper and the interested readers are referred to [11] for further details. Their computation on a digital computer is efficient since only logical expressions and elementary algebraic and transcendental functions are involved.

IV. NUMERICAL EXAMPLES AND SUPPORTING MEASUREMENTS

A method for analyzing the electromagnetic problem of a three-dimensional arbitrarily shaped body inside a rectangular waveguide has been presented. A Fortran IV computer program was written for the numerical testing of this approach. Measurements were also conducted to compare with the theoretical prediction. Several cases were studied and satisfactory results have been obtained. Validation of the theory and the computer program was achieved with numerical convergence tests as well as direct comparison with measured data, which included transmission-reflection characteristics and thermographic heating patterns.

Three cases, as shown in Fig. 3, are presented in this paper. All of the test cases consist of homogeneous dielectric bodies with rectangular side walls aligned with the waveguide walls. This choice of geometry conformal to the Cartesian coordinates is mainly for the sake of simplicity in data management and should not result in any significant loss of generality as was noted in the free space case [9]. For highly conductive obstacles, the surface curvature of the obstacle plays a more important role and therefore should be treated with greater discretion.

It was noted that the linear cell dimensions should be $\lambda/2$ (λ being the free space wavelength divided by the square root of the dielectric constant) or less in order to yield accurate data. This observation had been reported in the free space case studied by Livesay and Chen [9] and later by Hagmann et al. [12]. Fig. 4 shows good agreement in the reflection and transmission properties of Case B between a 12-cell calculation and the measured data using a model made of silica compound. A 12-cell calculation from Case A, being also a case of low dielectric constant, yields a power reflection coefficient of 0.114 at 2.65 GHz, dropping down to 0.035 at 3.5 GHz, which was verified experimentally with a paraffin wax model.

While 12 cells are sufficient for the calculation of Cases A and B, many more cells are needed for Case C, which has a high dielectric constant. Case C was originally intended to be a phantom model for simulating muscle
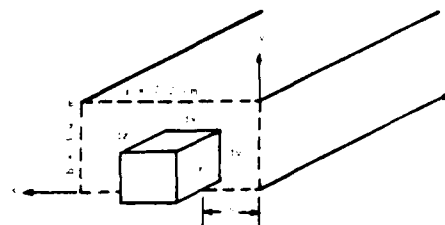
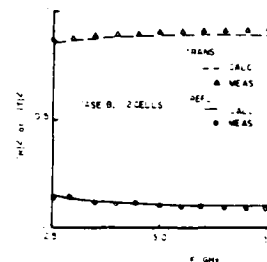Fig. 3. Configurations of the three cases studied.

Fig. 4. Comparison between calculated and measured reflection and transmission characteristics for Case B of Fig. 3 which is of low dielectric constant.
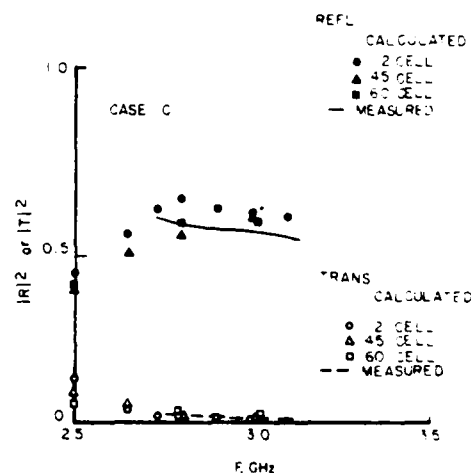

Fig. 5. Comparison between measurements and calculations of various numbers of cells for Case C of a high dielectric constant.

tissue. The model was made by mixing water, powdered polyethylene, and "super stuff," a modeling compound manufactured by Wham-O Co., San Gabriel, CA. The dielectric constant and loss tangent were then measured at various frequencies. There were difficulties in achieving and maintaining the desired dielectric properties of the phantom model and, as a result, only the repeatable measured data are shown in Fig. 5, in which comparisons are also made for three calculations using different numbers of subvolume cells. The measured data in Fig. 5
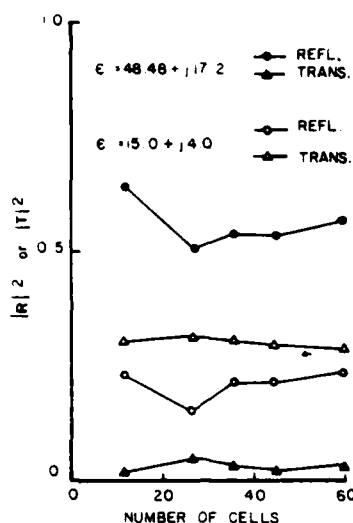
Fig. 6. Convergence of transmission and reflection properties for Case C with high and medium dielectric constants at 2.8 GHz.
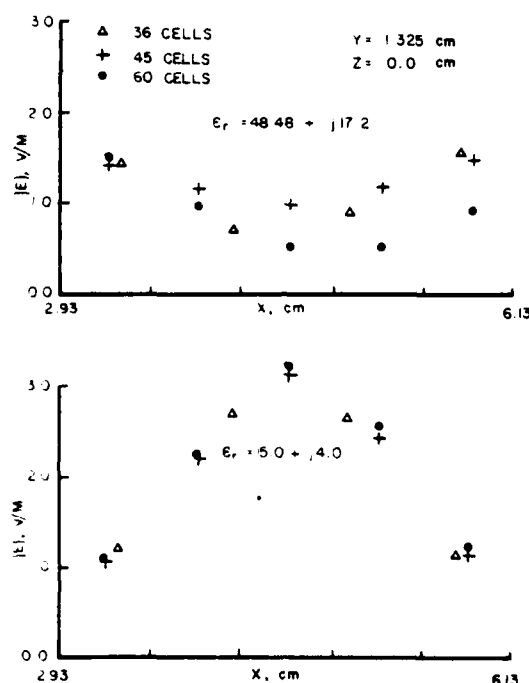

Fig. 7. Convergence of field distribution for Case C at 2.8 GHz with high and medium dielectric constants.

try of Case C with two values of complex dielectric constant. In Fig. 7, the field distribution inside the dielectric body is compared for various numbers of subvolume cells used in the calculation. It has been noted that the convergence of field intensity is related to the profile of the field. When the field varies slowly with the coordinates, convergence is rapid. Fig. 7 presents typical situations with moderately varying fields. The favorable influence of the lower dielectric constant on the convergence of the field distribution is clearly demonstrated.

Dielectric bodies of high dielectric constant require not only a larger number of cells but also a greater number of terms in the Green's function series. This is due to the fact that the distance between adjacent cells is small because of the smaller size of the cells. The attenuation of higher order modes, being independent of the dielectric constant, decreases when the distances between adjacent cells centers are shortened. As a result, the calculation cost for cases of high dielectric constants increases rapidly with an increase in dielectric constant.

V. CONCLUDING REMARKS

A general three-dimensional waveguide dielectric obstacle has been successfully treated by employing the moment method on an integral equation involving a dyadic Green's function. This general method can be applied to a number of waveguide problems. An immediate extension of this technique would be to ferromagnetic obstacles. For highly conductive obstacles a surface-type Green's function may be more desirable.

REFERENCES

[1] N. Marcuvitz, Waveguide Handbook. New York: McGraw-Hill, 1951.
[2] R. F. Harrington, Field Computation by Moment Method. New York: MacMillan, 1968.
[3] P. Silvester and Z. J. Csendes. "Numerical modeling of passive microwave devices," IEEE Trans. Microwave Theory Tech., vol., MTT-22, pp. 190-201, Mar. 1974.
[4] C. T. Tai, Dyadic Green's Functions in Electromagnetic Theory. Scranton, PA: Intext Educational Publishers, 1972.
[5] C. T. Tai, "On the eigen-function expansion of dyadic Green's functions," Proc. IEEE, vol. 61, p. 480, Apr. 1973.
[6] R. H. Lenox, O. P. Gandhi, J. L. Meyerhoff, and H. M. Gove, "A microwave application for in vivo rapid inactivation of enzymes in the central nervous system," IEEE Trans. Microwave Theory Tech., vol. MTT-24, pp. 58-61, Jan. 1976.
[7] Y. Rahmat-Samii, "On the question of computation of the dyadic Green's function at the source region in waveguides and cavities," IEEE Trans. Microwave Theory Tech., vol. MTT-23, pp. 762-765, Sept. 1975.
[8] R. E. Collin, "On the incompleteness of E and H modes in wave guides," Can. J. Phys., vol. 51, pp. 1135-1140, 1973.
[9] D. E. Livesay and K. M. Chen, "Electromagnetic fields induced inside arbitrarily shaped biological bodies," IEEE Trans. Microwave Theory Tech., vol. MTT-22, pp. 1273-1280, Dec. 1974.

agree reasonably with the calculation. The 12-cell configuration is obviously overly crude, yet the results are in gross agreement with those of finer configurations. Note that in the 45-cell calculation the y dimension of each cell is 0.8833 cm, which is about 0.52λ at 2.5 GHz and 0.68λ at 3.1 GHz. Convergence becomes more rapid when the linear dimensions of the subvolume cells decrease to $\lambda/2$ or less.

The rapidity of convergence of the present model approach is further illustrated in Figs. 6 and 7. Fig. 6 shows the calculated power reflection and transmission coefficients versus the number of cells used for the geome-

[10] I. S. Gradshteyn and I. W. Ryzhik, *Table of Integrals, Series and Products*. New York: Academic Press, 1965, pp. 38–40.

[11] J. J. H. Wang, "An analytical approach for use with waveguide enzyme-inactivation investigations," Final report, U. S. army Medical R & D Command Grant DAMD17-77-G-7422, Engineer-ing Experiment Station, Georgia Institute of Technology, Jan. 1978.

[12] M. J. Hagmann, O. P. Gandhi, and C. H. Durney, "Upper bound on cell size for moment-method solutions," *IEEE Trans. Micro-wave Theory Tech.*, vol. MTT-25, pp. 831–832, Oct. 1977.

Distribution List

12 Copies	Director (ATTN: SGRD-UWZ-AG) Walter Reed Army Institute of Research Walter Reed Army Medical Center Washington, D.C. 20012
4 Copies	HQDA (SGRD-AJ) Fort Detrick Frederick, MD 21701
12 Copies	Defense Documentation Center Attn: DDC-DCA Cameron Station Alexandria, Virginia 22314
1 Copy	Dean School of Medicine Uniformed Services University of the Health Sciences 4301 Jones Bridge Road Bethesda, Maryland 20014
1 Copy	Superintendent Academy of Health Sciences, US Army ATTN: AHS-COM Fort Sam Houston, Texas 78234

DATE
ILME